DOI: 10.1007/s40684-014-0040-1

Characteristics of Tapered Roller Bearing Subjected to Combined Radial and Moment Loads

Van-Canh Tong[1] and Seong-Wook Hong[1,#]

1 Department of Mechatronics, Kumoh National Institute of Technology, Daehak-ro 61, Gumi, Gyeongbuk, South Korea, 730-701
Corresponding Author / E-mail: swhong@kumoh.ac.kr, TEL: +82-54-478-7644, FAX: +82-54-478-7319

KEYWORDS: Tapered roller bearing(TRB), Radial load, Moment load, Contact force, Roller profile, Stiffness matrix

This paper investigates characteristics of the TRB such as displacements, contact forces between roller and inner ring, outer ring and flange, contact angle between roller and flange, load distribution along roller, and stiffness matrix, when the TRB is subjected to combined radial and moment loads. Understanding of these characteristics deserves attention for developing more sustainable TRBs. To this end, a five-degree-of-freedom model of TRB is employed. Unlike other studies, this paper takes TRB displacements as unknown variables and determines them by iteratively solving the roller and bearing equilibrium equations. A new formula for load variation in rollers is also presented by using an integration technique. The developed method is validated by comparing preliminary results with those from a reference program. The characteristics of TRBs subjected to combined radial and moment loads are simulated as a function of roller profile and rotational speed.

Manuscript received: July 3, 2014 / Revised: September 9, 2014 / Accepted: September 12, 2014

1. Introduction

Tapered roller bearings (TRBs) have a very noticeable feature of high load capacity against axial and radial loads. By nature, they can also support moment load. Hence, TRBs have been particularly considered in high load supporting applications such as automobile wheel hub assembly, gas turbine engine, milling machine spindle, etc.

Generally, rolling element bearing stiffness is an essential factor that affects dynamic behavior of rotating spindle. Because bearing stiffness is needed for analyzing the dynamic characteristics, for example, natural frequencies, mode shapes, and vibration amplitudes. The contact force and load distribution in roller of TRBs have been found to significantly influence their lubrication regimes, life time, or reliability. Therefore, accurate estimation of these characteristics is very valuable for better design so as to improve the performance and fatigue lives of TRBs, as well as predicting the performance of rotating systems supported by TRBs.

The fundamental theories of rolling element bearing were early outlined by Palmgren,[1] Jones[2] and Harris.[3] Studies on bearing were further extended by many researchers because of increasing demand toward higher efficiency. Regarding TRB, various investigations have been carried out that focused on determination of bearing characteristics. Andreason[4] analyzed the load distribution in a TRB under radial and axial loads. Although he effectively used a vector method to determine the elastic deformation of the roller and raceways, the centrifugal force and gyroscopic moment in TRB were not taken into account. Andreason's model[4] was further improved by Liu[5] so as to investigate the effect of given misalignment angles on the performance of TRB under combined loads. He considered the TRB characteristics under more realistic conditions, e.g., high speed, and actual direction of flange-roller contact force, which were neglected in the Andreason's research.[4] However the TRB displacements in the researches of both Liu[5] and Andreason[4] were assumed to be known a priori, rather than taken as unknown variables. This obviously limits the applicability of the model.

De Mul et al.[6,7] presented a general theory for determination of stiffness matrix and displacements of ball and roller bearings. Cretu et al.[8] used the de Mul's model to investigate the dynamic characteristics of TRBs under lubricating conditions. His study was confined to straight roller and raceway profiles. This implies impracticability because the roller or raceway profiles have been modified considerably to reduce the pressure concentration at the ends.[9]

Recently, Houpert improved the previous study[10,11] to perform an analytical approach for determining loads and moments of TRB as a function of given displacement with neglecting the influence of centrifugal and gyroscopic moment. A transition from point contact to

line contact between roller and raceways with the increasing load has also been considered.

In this paper, the characteristics of TRBs with modified roller profile such as displacements, contact forces between roller and inner ring, outer ring and flange, load distribution along roller, and stiffness matrix were investigated. First, based on the theory of de Mul et al.[6,7] an alternative integration method was proposed to replace the slicing technique. Subsequently, the developed model was verified by comparing the computational displacement and stiffness of the TRB at difference rotational speeds with those from a reference code.[12] Finally, the effects of combined radial and moment loads on the characteristics of TRB were reported. The presented results on TRBs subjected to practical loading conditions are believed to contribute to developing more sustainable TRBs.

2. Derivation of Dynamic Equations for TRB

In order to obtain bearing equilibrium equations, it is necessary to solve the equilibrium equations of all rollers which are related to roller contact forces. The derivation of these equations was clearly presented by de Mul et al.[6,7] and briefly summarized below.

2.1 Assumptions

The following assumptions are made for reducing the complexity of analysis: (1) Loads generated by the cage and frictions are neglected; (2) The elastic deformation appears only at the contact location between roller and bearing rings; (3) Axial preload is large enough to allow no gaps appear between the roller and raceways.

2.2 TRB Coordinate Systems, Loads and Displacements

Fig. 1 shows the TRB coordinate systems and loading. The bearing global coordinate system (x, y, z), external force vector $\{F\}^T = \{F_x, F_y, F_z, M_x, M_y\}$ and the inner ring displacement vector $\{\delta\}^T = \{\delta_x, \delta_y, \delta_z, \gamma_x, \gamma_y\}$ are shown in the Fig. 1(a). In the local cylindrical coordinate system (r, ϕ, z) which is fixed with a particular roller at azimuth angle ϕ, the inner ring contact force and displacement vectors are $\{Q\}^T = \{Q_r, Q_z, M\}$ and $\{u\}^T = \{u_r, u_z, \theta\}$, respectively. The roller displacement is expressed by vector $\{v\}^T = \{v_r, v_z, \psi\}$ (Fig. 1(b)). The relationship between vectors $\{u\}$ and $\{\delta\}$ is stated as

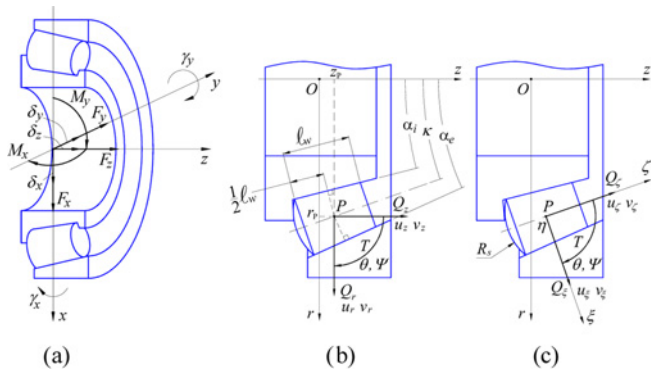

Fig. 1 Bearing coordinate systems and loading. (a) (x, y, z) global coordinate system, (b) (r, ϕ, z) cylindrical coordinate system, (c) (ξ, ζ, η) inclined coordinate system

$$\{u\} = [R\phi].\{\delta\} \tag{1}$$

where $[R\phi]$ is the global transformation matrix,

$$[R\phi] = \begin{bmatrix} \cos\phi & \sin\phi & 0 & -z_P\sin\phi & z_P\cos\phi \\ 0 & 0 & 1 & r_P\sin\phi & z_P\cos\phi \\ 0 & 0 & 0 & -\sin\phi & \cos\phi \end{bmatrix} \tag{2}$$

The contact load vector $\{Q\}$ depends on both the roller and inner ring displacements, i.e.,

$$\{Q\} = \{Q(\{u\},\{v\})\} \tag{3}$$

In the inclined coordinate system (ξ, ζ, η) (Fig. 1(c)), the corresponding contact force and displacement vectors indexed by subscript κ are $\{Q_\kappa\}^T = \{Q_\xi, Q_\zeta, M\}$, $\{u_\kappa\}^T = \{u_\xi, u_\zeta, \theta\}$, and $\{v_\kappa\}^T = \{v_\xi, v_\zeta, \psi\}$. By using local transformation matrix $[K]$, one can get

$$\{Q_\kappa\} = [K]\cdot\{Q\} \tag{4}$$

$$\{u_\kappa\} = [K]\cdot\{u\} \tag{5}$$

$$\{v_\kappa\} = [K]\cdot\{v\} \tag{6}$$

where

$$[K] = \begin{bmatrix} \cos\kappa & \sin\kappa & 0 \\ -\sin\kappa & \cos\kappa & 0 \\ 0 & 0 & 1 \end{bmatrix} \tag{7}$$

2.3 Roller-Raceway Contact Force

The contact force per unit length between roller and raceway was represented, by Andreason,[4] as

$$q_a = c_a\delta_a^{10/9} \tag{8}$$

The total contact force between roller and raceway can be determined by applying integration operation

$$Q_a = \int_0^{l_w} q_a dx_a \tag{9}$$

where $a = i, e$ indicates the inner and outer ring. With the aim of determining the elastic contact compression (δ_a), it is necessary to decompose the contact force into those of subsections corresponding to the roller profile. For example, in case of chamfered roller, three subsections denoted by Q_{a1}, Q_{a2} and Q_{a3} are needed as illustrated in Fig. 2. δ_a at an arbitrary position of each subsection will be defined. First, to consider the straight roller profile (Fig. 3), the contact compression at a distance x_a ($0 \le x_a \le l_w$) is calculated by

$$\delta_{a0} = \delta_{a(fr)} - \frac{\delta_{a(fr)} - \delta_{a(re)}}{2} x_a\,,\ a = i, e \tag{10}$$

where $\delta_{a(re)}$ and $\delta_{a(fr)}$ are the compressions at the rear end and front end of the straight roller, respectively. Subsequently, the gaps developed along each subsection in the modified roller are found as

$$g_{a1} = (l_{w1} - x_a)\tan\gamma \quad (0 \le x_a \le l_{w1}) \tag{11}$$

$$g_{a2} = 0 \quad (l_{w1} \le x_a \le l_{w2}) \tag{12}$$

$$g_{a3} = (x_a - l_{w2})\tan\gamma \quad (l_{w2} \le x_a \le l_w) \tag{13}$$

The existence of the gaps would reduce the actual contact compression. Thus, the real compression between the roller and raceway is

$$\delta_{ak} = \delta_{a0} - g_{ak} \quad (k = 1,2,3) \tag{14}$$

By substituting Eq. (14) into Eq. (8), the contact force of each subsection is defined. Finally, the total contact force will be obtained

$$Q_a = Q_{a1} + Q_{a2} + Q_{a3} \tag{15}$$

2.4 Roller-Flange Contact Force

The flange-roller end contact is subjected to a classical Hertzian point contact between a flat flange and a spherical roller end. The roller and flange contact force is obtained from

$$Q_f = c_f\, \delta_f^{1.5}; (\delta_f > 0) \tag{16}$$

where c_f and δ_f are the contact constant and the compression between the roller sphere end and flange, respectively.

2.5 Roller and Bearing Equilibrium Equations

From Fig. 2, the equilibrium equations of a roller are written as

$$\begin{cases} (Q_i - Q_e)\cos\varepsilon + Q_f \sin\mu_0 + F_c \cos\kappa = 0 \\ -(Q_i + Q_e)\sin\varepsilon + Q_f \cos\mu_0 - F_c \sin\kappa = 0 \\ M_i - M_e + Q_f \zeta_{cs} \sin\mu - F_c \zeta_c \cos\kappa - M_g = 0 \end{cases} \tag{17}$$

where F_c and M_g are the roller centrifugal force and gyroscopic moment. M_i and M_e, the moments about η axis, are caused by contact forces between roller and inner and outer raceways, respectively.

$$M_a = \int_0^{l_w} c_a \delta_a^{10/9} \left(\frac{l_w}{2} - x_a\right) dx_a, \; a = i, e \tag{18}$$

Once the inner ring displacement $\{u\}$ is known, the roller displacement $\{v_\kappa\}$ can be found by solving the roller equilibrium Eq. (17). An iterative Newton-Raphson method is utilized to solve this set of non-linear equations.

$$\{Q_\kappa\} = \begin{Bmatrix} Q_\xi \\ Q_\zeta \\ M \end{Bmatrix} = \begin{Bmatrix} -Q_i \cos\varepsilon - Q_f \sin\mu_0 \\ Q_f \sin\varepsilon - Q_f \cos\mu_0 \\ -M_i - Q_f \zeta_{cs} \sin\mu \end{Bmatrix} \tag{19}$$

After all the roller equilibrium equations are completely solved, the contact load vector of inner ring at a particular roller is easily found as shown in Eq. (19). The inner ring contact load at each roller location is then transformed into the global coordinate system in order to find the bearing equilibrium, the resultant force vector is

$$\{f\} = [R\phi]^T \cdot \{Q\} \tag{20}$$

Summation of all equivalent forces $\{f\}$ and external force $\{F\}$ acting on the inner ring gives the global equilibrium equations as

$$\{F\} + \sum_{j=1}^{n_r} [R\phi]_j^T \cdot \{Q\}_j = \{0\} \tag{21}$$

This set of equilibrium equations with unknowns $\{\delta\}^T = \{\delta_x, \delta_y, \delta_z, \gamma_x, \gamma_y\}$ are non-linear so are the roller equations. Thus, the Newton-Raphson method is applied as a solution. From the above descriptions, an overall computational flowchart for TRB is given (see Appendix).

2.6 Bearing Stiffness Matrix

Determination of bearing stiffness matrix is made possible by.[6,7]

$$[k_b] = \left[\frac{\partial\{F\}}{\partial\{\delta\}^T}\right] \tag{22}$$

From the bearing equilibrium Eq. (21), the bearing stiffness matrix is rewritten as

$$[k_b] = -\sum_{j=1}^{n_r} [R\phi]_j^T \cdot \frac{\partial\{Q\}_j}{\partial\{u\}_j^T} \cdot [R\phi]_j \tag{23}$$

3. Numerical Example

A MATLAB program was developed to determine the characteristics of TRB. A TRB of type 30208A with properties given in Table 1 was selected in the entire simulation work.

3.1 Model Verification

The TRB is loaded by combined axial, radial and moment loads being F_z = 45,000 N, F_x = 10,000 N and M_y = 70 Nm, respectively. The rotational speed of TRB (n) is selected from 5,000 rpm to 25,000 rpm.

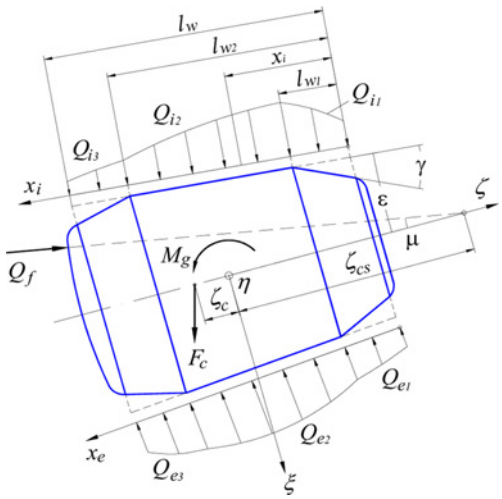

Fig. 2 Free-body diagram for a roller

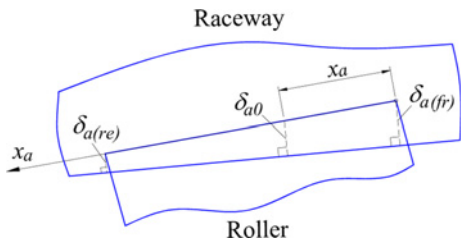

Fig. 3 Contact compression of straight roller

Fig. 4 shows the TRB displacement, the centrifugal force and gyroscopic moment of roller as a function of n. From Fig. 4(d), both the centrifugal force (F_c) and gyroscopic moment (M_g) considerably increase with the increase of bearing speed. Because F_c and M_g are taken into account, the axial displacement of bearing (δ_z) decreases by 0.988% (Fig. 4(a)). The angular (γ_y) and radial displacements (δ_x) are less affected by the speed of bearing than δ_z, since γ_y and δ_x increase by 0.083% and 0.075% as seen in Figs. 4(b) and 4(c). Fig. 4 also shows a good match between the computation and commercial code results, in which the maximum differences between them are 0.21%, 1.7% and 5.01% in case of δ_z, δ_x and γ_y, respectively.

Table 1 Geometry parameters of TRB

Parameter	Unit	Value
Number of row		1
Number of rollers (n_r)		17
Bearing bore diameter	mm	40.0
Bearing outer diameter	mm	80.0
Bearing total width	mm	19.75
Roller total length (l)	mm	12.45

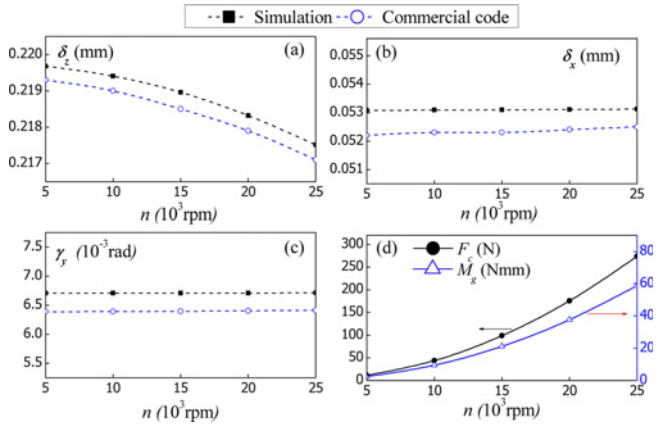

Fig. 4 The TRB characteristics vs rotational speed (F_z = 45,000 N, F_x = 10,000 N and M_y = 70 Nm). (a) Axial displacement, (b) Radial displacement, (c) Angular displacement, (d) Centrifugal force and gyroscopic moment

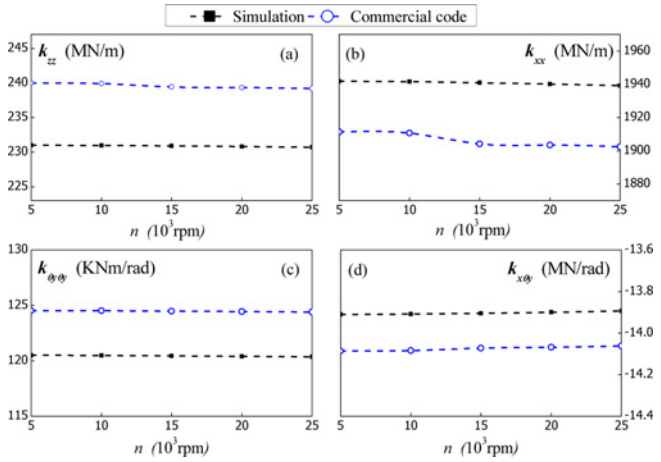

Fig. 5 Effects of rotational speed on TRB stiffness (F_z = 45,000 N, F_x = 10,000 N and M_y = 70 Nm). (a) Axial stiffness, (b) Radial stiffness, (c) Angular stiffness, (d) Coupling stiffness

Fig. 5 illustrates the effects of n on the stiffness of the sample TRB. The bearing speed increases resulting in a decrease of the axial stiffness (k_{zz}), radial stiffness (k_{xx}), angular stiffness ($k_{\theta y\theta y}$) but an increase in coupling stiffness ($k_{x\theta y}$). As expected, the simulation results in Fig. 5 prove a good agreement with commercial code results when the greatest discrepancies are 3.75 %, 1.94 %, 3.25 % and 1.25% in terms of k_{zz}, k_{xx}, $k_{\theta y\theta y}$ and $k_{x\theta y}$ coefficients, respectively.

Fig. 6 demonstrates the contact characteristics of rollers with the inner ring. As can be seen in Figs. 6(a) and 6(b), the roller-flange contact force (Q_f) gradually increases with regard to n, while the contact force between roller and inner ring (Q_i) tends to decrease. The maximum variation of Q_f and Q_i recorded at position angle $\phi = 180^o$ are 6.15 % and 2.65 %, respectively. It can be seen that Q_i and Q_f are high sensitive to the speed variation in high speed range.

Regarding the roller-outer ring raceway contact force (Q_e) shown in Fig. 6(c), Q_e is almost independent on the rotational speed. This is due to the fact that the applied axial load on the bearing remains constant yet large enough to keep the roller and raceways in a perfect contact throughout the full contact length during operation. Summation of projection of all roller-outer ring contact forces into the horizontal axis must be equal to the axial load[5]. Figs. 6(a) to 6(c) also suggest that all the contact forces between rollers and raceway of the lower half of TRB (at the azimuth angle ϕ = 0° ~ 90° and 270° ~ 360°) are higher than those of the upper part (ϕ = 90° ~ 270°). This fact is caused by the effect of the applied radial load.

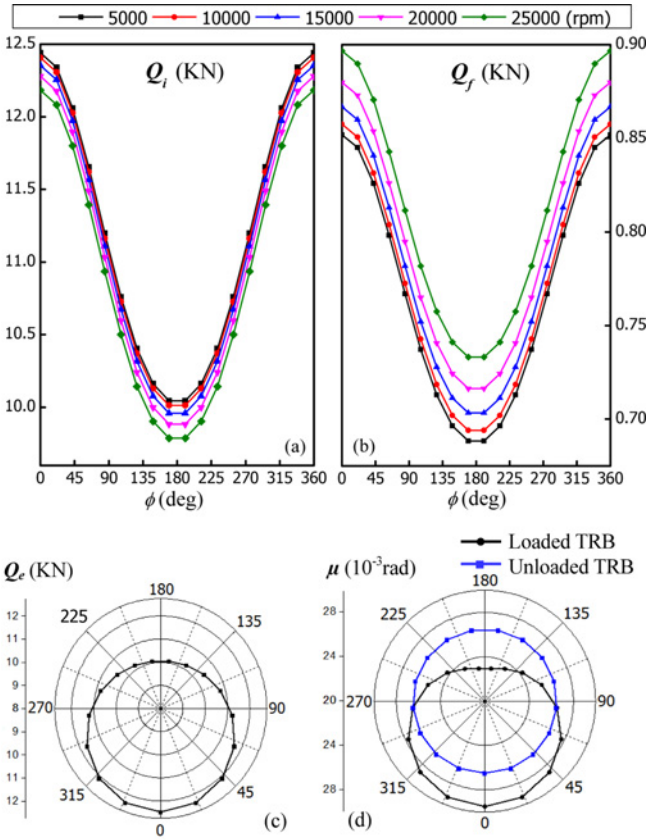

Fig. 6 Roller-inner ring contact characteristics (F_z = 45,000 N, F_x = 10,000 N and M_y = 70 Nm). (a) Roller-inner ring raceway contact force, (b) Roller-flange contact force, (c) Roller-outer ring raceway contact force, (d) Roller-flange contact angle

Roller and flange contact angle (μ) at each roller is indicated in Fig. 6(d). Because all rollers exhibit a negligible change in μ with regard to rotational speed, the contact angle at only one speed of 25,000 rpm is shown. It is observed that, unlike the unloaded bearing, μ decreases in the rollers of the upper half of bearing but increases in the rollers of the lower half in case of loaded bearing. This can be explained by the existence of inner ring displacement when the bearing is loaded as shown in Figs. 4(a), 4(b) and 4(c). Therefore, it is necessary to consider the actual direction of flange contact force for investigating the characteristics of TRB.

Distribution of contact forces between roller and inner, and roller and outer raceways are calculated at the rotational speed of 25,000 rpm and represented in Fig. 7. Due to the effect of TRB misalignment angle on a specific roller, load distribution of the roller # 1 ($\phi = 0^o$) shows that more portion of the front end of the roller get into contact with the raceway than those of the rear end. On the contrary, the higher load distribution appears at the rear end of roller # 9 ($\phi = 169.4^o$). Nearly same amount of load along the contact length is found in roller # 5 ($\phi = 84.7^o$).

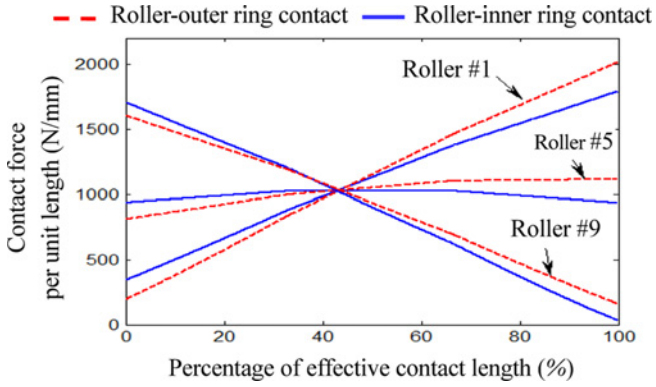

Fig. 7 Contact force distribution along rollers (F_z = 45,000 N, F_x = 10,000 N, M_y = 70 Nm and n = 25,000 rpm)

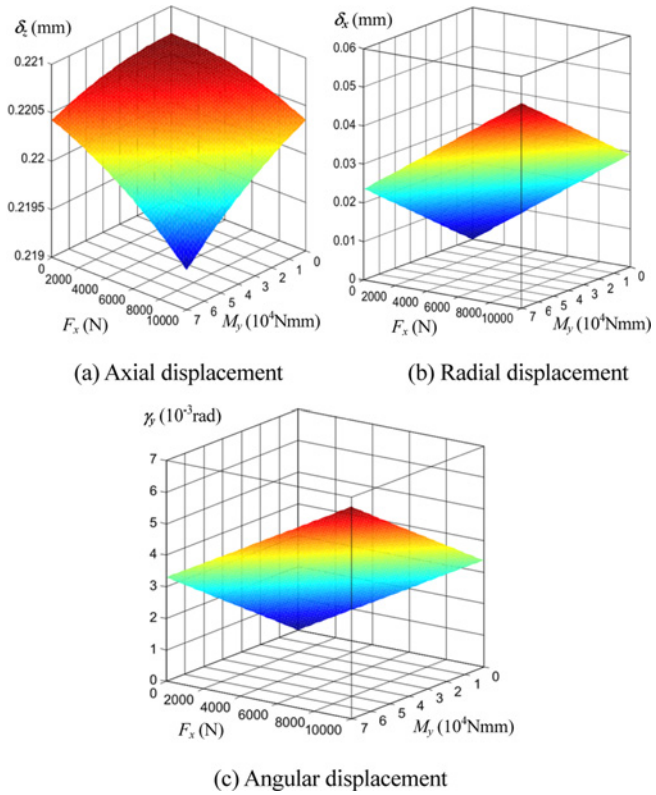

Fig. 8 Displacements of TRB and combined radial and moment loads dependence (F_z = 45,000 N and n = 10,000 rpm)

3.2 Effects of Combined Loads on the Displacement and Stiffness of TRB

In this section, the effects of combined radial and moment loads on the characteristics of TRB will be discussed. Radial load (F_x) and moment load (M_y) are varied from 0 to 10,000 N and 0 to 70 Nm, respectively, while the axial preload and rotational speed are kept constant at 45,000 N and 10,000 rpm. The TRB displacements as a function of radial and moment loads are demonstrated in Fig. 8. Fig. 8(a) shows that δ_z is reduced with increasing F_x or M_y. Contrarily, the displacements δ_x and γ_y increase linearly with F_x, and M_y as in Figs. 8(b) and 8(c). From Fig. 8(c), it is noteworthy that γ_y is present even though only radial and axial loads are applied on the bearing.

Fig. 9 shows the effects of combined radial and moment loads on the TRB stiffness. It is observed that k_{zz}, k_{xx}, $k_{\theta_y\theta_y}$ show a similar behavior with respect to combined loads. However, $k_{x\theta_y}$ is negative and increases steadily with increasing applied loads. It should be noticed here that the higher applied loads come with the greater changes in stiffness. Similar results were also reported earlier for angular contact ball bearing.[13]

4. Conclusions

Analysis on the TRB characteristics has been performed with regard to combined loads and high rotational speed. From the simulation results, the following conclusions can be drawn:

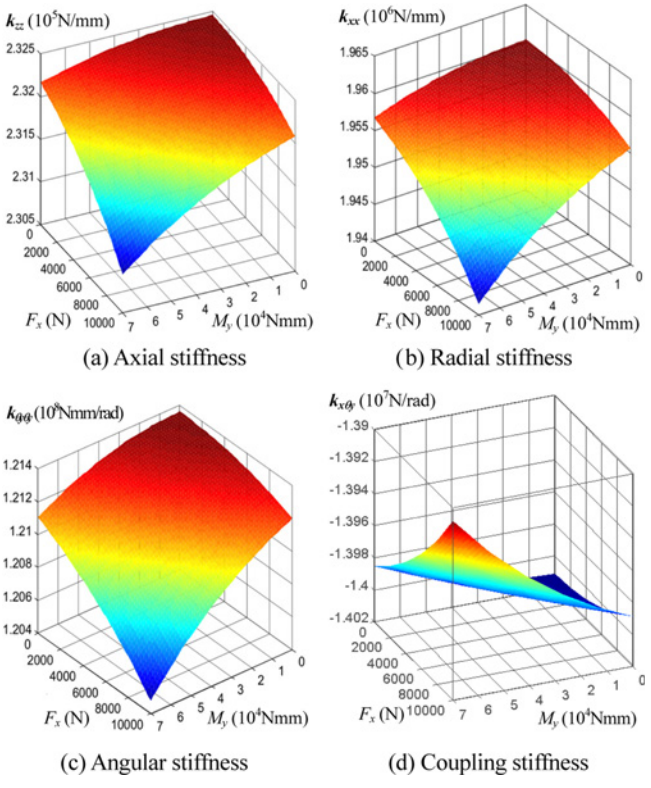

Fig. 9 Stiffness of TRB (F_z = 45,000 N and n = 10,000 rpm)

1) Increase of TRB rotational speed results in decrease of the axial displacement, but increase of the radial and angular displacements of TRB. It also causes the axial, radial, and angular stiffness coefficients to decline and the coupling stiffness coefficient to grow up.

2) Increase of TRB rotational speed reduces the contact force between roller and inner ring raceway, but increases the roller-flange contact force. The roller-outer ring raceway contact force and the contact angle between roller and flange are almost independent of the rotational speed.

3) The displacement and stiffness of TRB are greatly changed under significant radial and moment loads. Radial and moment loads show the similar effects on the displacement and stiffness of TRB.

4) Radial and angular displacements of TRB show an almost linear relation with radial and moment loads, whereas the axial displacement decreases non-linearly with the increase of combined loads.

5) Regardless of the non-linear characteristics of displacement and stiffness of TRB, the superposition principle can provide a good approximation for the TRB characteristics under combined loads.

6) A new method for determining roller and raceway contact force has been introduced in the study. The presented modeling and analysis method will contribute to developing more sustainable TRBs.

ACKNOWLEDGEMENT

This research is financially supported by the Korea Institute of Machinery and Materials.

REFERENCES

1. Palmgren, A., "Ball and Roller Bearing Engineering," Philadelphia: SKF Industries Inc., Vol. 1, 1959.
2. Jones, A., "A General Theory for Elastically Constrained Ball and Radial Roller Bearings under Arbitrary Load and Speed Conditions," Journal of Fluids Engineering, Vol. 82, No. 2, pp. 309-320, 1960.
3. Harris, T. A., "Rolling Bearing Analysis," 2nd Ed., John Wiley & Sons, New York, 1984.
4. Andreason, S., "Load Distribution in a Taper Roller Bearing Arrangement Considering Misalignment," Tribology, Vol. 6, No. 3, pp. 84-92, 1973.
5. Liu, J. Y., "Analysis of Tapered Roller Bearings Considering High Speed and Combined Loading," Journal of Tribology, Vol. 98, No. 4, pp. 564-572, 1976.
6. Liu, J., De Mul, J. M., Vree, J. M., and Maas, D. A., "Equilibrium and Associated Load Distribution in Ball and Roller Bearings Loaded in Five Degrees of Freedom While Neglecting Friction-Part II: Application to Roller Bearings and Experimental Verification," Journal of Tribology, Vol. 111, No. 1, pp. 149-155, 1989.
7. Liu, J., De Mul, J. M., Vree, J. M., and Maas, D. A., "Equilibrium and Associated Load Distribution in Ball and Roller Bearings Loaded in Five Degrees of Freedom While Neglecting Friction-Part II: Application to Roller Bearings and Experimental Verification," Journal of Tribology, Vol. 111, No. 1, pp. 149-155, 1989.
8. Creju, S., Bercea, I., and Mitu, N., "A Dynamic Analysis of Tapered Roller Bearing under Fully Flooded Conditions Part 1: Theoretical Formulation," Wear, Vol. 188, No. 1, pp. 1-10, 1995.
9. Rahnejat, H. and Gohar, R., "Design of Profiled Taper Roller Bearings," TRIBOLOGY International, Vol. 12, No. 6, pp. 269-275, 1979.
10. Houpert, L., "An Enhanced Study of the Load-Displacement Relationships for Rolling Element Bearings," Journal of Tribology, Vol. 136, No. 1, pp. 011105-011116, 2014.
11. Houpert, L., "A Uniform Analytical Approach for Ball and Roller Bearings Calculations," Journal of Tribology, Vol. 119, No. 4, pp. 851-858, 1997.
12. Schaeffler Technologies, "BEARINX-Online Shaft Calculation," http://www.schaeffler.de/content.schaeffler.de/en/products_services/inafagproducts/calculating/bearinxonline/bearinx_online.jsp (Accessed 17 September 2014)
13. Jorgensen, B. R. and Shin, Y. C., "Dynamics of Spindle-Bearing Systems at High Speeds Including Cutting Load Effects," Journal of Manufacturing Science and Engineering, Vol. 120, No. 2, pp. 387-394, 1998.

APPENDIX: Computational Procedure